ORNITHOPTER TESTBED TO DISCOVER FORCES PRODUCED BY FLAPPING WING MOVEMENT

A Major Qualifying Project Report

Submitted to the Faculty of the

Worcester Polytechnic Institute

In partial fulfillment of the requirements for the

Degree of Bachelor of Science

By

Carlos Berdeguer

Hanna Schmidtman

Austin Waid-Jones

Advisor: Marko Popovic (PH, BME, RBE)

Co-advisor: Cagdas Onal (ME, RBE)

Abstract

An ornithopter is a biologically inspired robot that produces lift by flapping its wings. Many hobby-sized ornithopters currently exist, however, large-scale models have been historically unsuccessful. Continuing last year's MQP, a new testbed was developed to replicate various wing stroke patterns and measure relevant forces. A custom four bar linkage mechanism, capable of generating multiple coupler curves, was created to manually adjust the wing trajectory. The testbed utilizes load cells, an encoder, IMU, and a LabVIEW interface to gather forces and corresponding position data. In future projects, this testbed can be used to test and develop optimal wing design and wing tip pattern for ornithopter innovation.

Acknowledgements

We would like to thank the following individuals for their outstanding willingness to contribute to the success of this project: Members of Popovic Labs; Peter Hefti, for lending us the amplifiers and Data Acquisition block for several months; Robert Boisse, for advising us and giving us the correct wires for our needs; Professor Fred Hutson, for lending us weights and Logger Pro force scales; Roger Steele, for always unlocking the machine shop; and Seth Pierson, for the use of his personal IMU and power supply and extensive help with LabVIEW.

Table of Contents

Table of Figures

Table of Tables

Chapter 1: Introduction

Mankind has fixated on the simulation of bird flight for centuries. Throughout history, many stories allude to the creation of ornithopters, mechanisms that produce lift by flapping wings. In the Greek mythological tale of Icarus and Daedalus, Daedalus constructed a mechanism of wax and feathers to allow them to fly like birds using their arms. Roger Bacon, a twelfth century physicists, described a device "for flying…. such that a man sitting in the middle of it and turning a crank shall cause artificial wings to beat the air after the manner of a bird's flight [1]." Even Leonardo da Vinci, the Renaissance polymath, was particularly interested in the idea of human mechanical flight. He produced a publication called the Codex on the Flight of Birds, in which da Vinci created more than 500 sketches of flying machines and mechanisms of bird flight [2]. This inspiration continues today in a study called biomimicry.

According to the Biomimicry Institute, "biomimicry is an approach to innovation that seeks sustainable solutions to human challenges by emulating nature's time-tested patterns and strategies [3], [4]." Although flight has been achieved by fixed- and rotary-winged vehicles, the ability to fly by flapping wings is still limited to birds, bats, and insects. The purpose of the Ornithopter Testbed Major Qualifying Project is to create a mechanism evaluate the forces involved in flapping flight.

The MQP team designed and built a mechanism to replicate the flapping behavior of different styles of bird flight. To accomplish this, the driving mechanism of the testbed was a four-bar linkage with a custom component to achieve many coupler curves. This enabled the various wing tip patterns to be produced and could be altered manually with little effort. The wing of the system is attached at the coupler point to "flap" in rotational patterns. The driving mechanism was located on a multi-tiered platform supported by load cells. These load cells measured the deflection of the platform under the load of the flapping wing. The measurements, lift force and corresponding rotational position, were recorded in LabVIEW and analyzed in Microsoft Excel.

The results of this study will be used to understand the forces created during wing flap. Utilizing this information, future groups will be able to design lighter and stronger wings towards the goal of large-scale ornithopters.

Chapter 2: Background Research

2.1 Inspiration from Nature

Animals on Earth must overcome gravity in order to move. Terrestrial creatures attempt to minimize the amount of work necessary to overcome this gravity and move as efficiently as possible. Birds must produce enough power to support their weight and additional drag forces. This power is produced by flapping their wings.

In order to fly, birds flap their wings. The wings are made of a network of muscles. The flapping of the entire wing is caused by two main muscles: the pectoralis and supracoracoideus. The pectoralis and supracoracoideus form an agonist-antagonist pair, when one muscle is contracted the other relaxes. There is also a series of smaller intrinsic and extrinsic muscles that supinate the wing and change the airfoil shape of the wing. However, these muscles are not responsible for flapping and therefore not considered to produce power to generate flight. Most power is generated by the pectoralis muscles [5],[6].

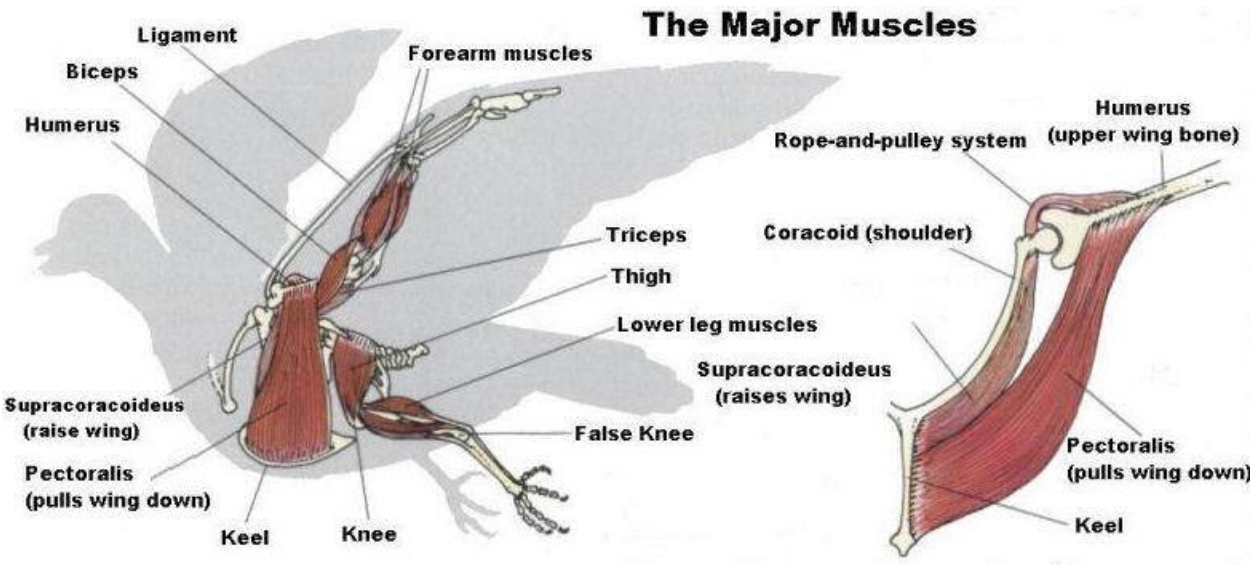

FIGURE 1 ANATOMICAL ILLUSTRATION OF BIRD MUSCLES [7]

The pectoralis is a large muscle that constitutes approximately 8-11% of a bird's total body mass. The pectoralis contracts to create the downstroke phase of flapping as well as pronates the wing. The muscle consists of relatively long fascicles that shorten up to 42% of their length. Activation of the pectoralis occurs late in the up-stroke, and creates peak forces early into the down-stroke. According to several in vivo experiments, Biewener notes that the resulting forces "are estimated to be less than 40-

60% of the peak isometric force that the muscle can generate." The pectoralis muscle pulls the wing down and its complementary muscle, the supracoracoideus, pulls the wing up [5].

The supracoracoideus is much smaller than the pectoralis (about one-fifth of the mass), and accounts for about 2% of a bird's body mass. This muscle elevates and supinates the wing during upstroke. The supracoracoideus is activated late during the down stroke just before wing reversal and mirrors the actions of the pectoralis. The forces peak early into the upstroke. The supracoracoideus plays roles in deceleration and re-accelerating of the wing during the transitions between upstroke and down stroke, and supinates the wing. This muscle is also especially active during slow to moderate speeds of flight and during hovering [6]. The rapid supination is important for short-duration upstroke. This short-duration upstroke is responsible for positive lift generation in birds with wing-tip reversal. "Rapid supination of the wing to initiate upstroke in rufous hummingbirds is key to this species' ability to generate positive upstroke lift, which has been estimated to be 25-33% of their total lift production." The supination of the wing by the supracoracoideus is important because it maximizes the down stroke lift production and is an important feature of active flapping flight [5].

2.2 Mechanical Flight

Currently, there are a few types of flight that have been engineered, most prominent are helicopters and airplanes. Each of these forms of flight has its advantages and disadvantages, work very differently from each other, and have different applications.

Rotorcraft

A helicopter uses overhead blades which rotate to allow vertical flight. These overhead blades are designed as airfoils, a wing with a curved top and a straight bottom, this design pushes air towards the ground producing lift. The blades are controlled by the pilot who can change the angle to create more or less pitch. During liftoff the pilot increases the pitch of the blades so that the lift force produced is greater than the weight of the helicopter, and allows it to fly. The pitch can be changed so that the lift produced equals the weight of the helicopter, this will allow it to hover at a 'fixed' height, if the pitch is decreased the weight of the craft will be more than that of the lift produced which will allow for descent. To control the direction of flight, the pilot uses a device called 'cyclic pitch control' that tilts the rotor blades slightly in the direction desired. This tilt on the blades will cause the lift produced to aim at an angle with respect to the ground that will provide both lift and thrust. During this movement the entire helicopter will tilt in that direction. Due to all of these movements, the main body of the helicopter would

normally rotate in the opposite direction of the rotating blades, but this is counteracted by a second propeller, most commonly known as a tail rotor [8].

Fixed-Wing Flight

Airplanes have two ways of movement, either forward or up and the combination of both allows for 'normal' movement of the plane. An airplane moves upwards as a result of its wing design, specifically the airfoils. A proper airfoil shape consists of a curved upper surface and a flat lower surface. The airfoil shape causes air to move further and faster on the upper surface, thus creating a low pressure area above the wing, causing lift. The airfoils are dependent on the angle of attack to produce lift. The angle of attack controls the angle that the air is directed with respect to the horizon, when angled downwards lift is produced. Planes move forward in a variety of ways, they may use traditional propeller engines, jet engines, or just glide through the air without an engine [9].

2.3 Existing Testbeds

Ornithopter test beds that specifically test for lift are rare. Most testbeds that ornithopter enthusiasts use are crude machines that are directly attached to a fully built ornithopter that allow movement. While moving, the ornithopter's thrust or lift is measured. This means that to test each wing design, the ornithopter must be disassembled and reassembled with the new design to be able to test its effectiveness.

The current testbeds connect to an ornithopter by a clamp on the underside which is then connected to a scale (such as a grocery scale or a load cell) to show force produced [10].

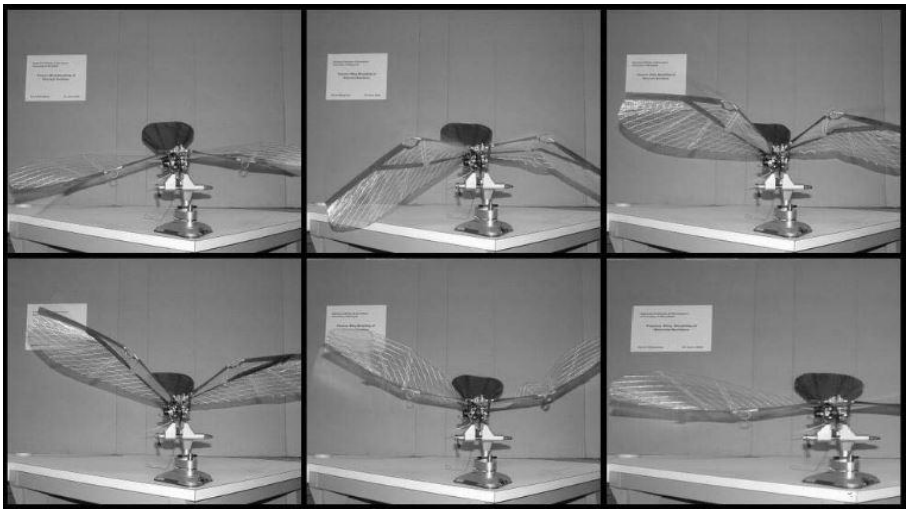

FIGURE 2 STATIC LIFT TEST [10]

Morpheus Laboratory

A group at University of Maryland A. James Clark School of Engineering has developed an advanced ornithopter testbed to develop accurate dynamical models of flapping flight. Morpheus Laboratory has taken a stock remote controlled ornithopter, Odyssey, weighing 450 g with a wingspan of 4 ft. and loaded it with advanced avionics. These avionics include GPS, MEMS magnetometers, gyroscopes, and accelerometers capable of recording data such as movement of center of gravity, inertia, orientation, and velocity. The primary disadvantage of this testing setup is that an existing ornithopter must be used, this does not allow for testing of fundamental components before creating an optimal ornithopter [11].

FIGURE 3 UNIVERSITY OF MARYLAND MORPHEUS TESTBED

Previous MQP

The goal of past Major Qualifying Project (MQP) was to make a test bed that would create measurable forces and allow for the testing of different wings. The previous MQP team attempted to recreate the forces experienced by two wings oriented horizontally, allowing them to run against the drag force that wings typically experience. To accurately measure the forces present, the team set up various sensors and a camera to track the wing location during operation. With this, the group was able to pinpoint the forces acting on the wings at the relative positions that the wings were in [12].

The previous MQP had several restrictions that did not allow for accurate force measurements, and a limited number of forces that could be measured. The wing moved in a simple back and forth motion that did not accurately generate forces comparable to those acting on a bird's wings. The sensor data that was gathered contained too much noise. The motor that was used to power this test bed was insufficient and caused stalling during operation [12].

The current MQP team used some ideas from the previous year and improved on the test bed concept. The new test bed was positioned in a vertical orientation so that gravity would act on the wing, producing more accurate force measurements. The wing mount could accommodate any wing design so long as size and weight were taken into consideration. The mounting system for the wing was modular which allowed for different wing tip patterns to be used during testing. These patterns were compared to reach the most efficient wing design and pattern combination. The sensors were calibrated and connected

to an amplifier to reduce aliasing (noise) created during operation to obtain clear data. The motor that was operating the test bed was researched and combined with a gearbox to give the best torque-to-speed ratio that could be obtained.

Chapter 3: Methodology

3.1 Objectives

To determine the design of the ornithopter test environment, the MQP team collaborated with the project director, Professor Marko Popovic. Together, a set of goals were established that the group expected the device to accomplish.

1. Design and build a test platform capable of measuring wing strokes at a speed of 2 Hz.
2. Test platform able to create multiple biologically inspired flapping trajectories.
3. Trajectories of test platform able to be manually adjustable with the aid of basic hand tools.
4. Test platform measures the moments and force of lift generated by the wings.

3.2 Conceptual Design

To accomplish these goals, the MQP team needed to build a relatively simple system with a way to adjust the flapping pattern between tests. The team determined that a four-bar linkage would be the most elegant solution to the variable wing pattern goal. A four-bar linkage is a basic mechanical system that can create a broad variety of output curves. These curves are dependent on the lengths of each of the bars and the angle between the coupler point and the floating link. By using slotted links and a floating link with multiple coupler points that resembles a protractor, the device would be capable of numerous coupler curves. The group decided on three distinct wing stroke patterns to use; a vertical, pure-lift curve, a teardrop shaped curve, and a figure-eight curve. Using the four-bar linkage program, Linkages, the MQP team was able to find the measurements for the selected curves.

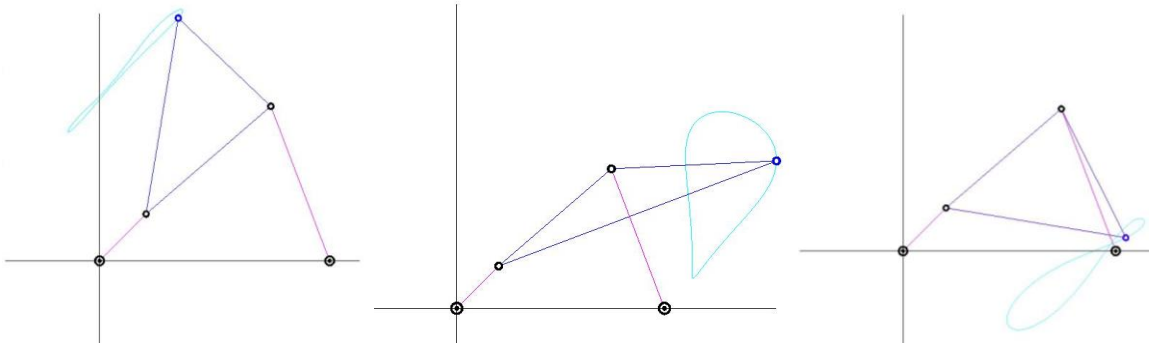

A B C

FIGURE 4 ILLUSTRATIONS OF THREE COUPLER CURVES (A, B, C) USED FOR WING TIP PATTERNS. TOP LEFT: POSITION 1, ALMOST LINEAR. TOP RIGHT: POSITION 2, "TEAR DROP ". BOTTOM: POSITION 3, "FIGURE-EIGHT".

The main shaft of the wing, the wing-bone, would drive the wing with a connection at the coupler point on the four-bar linkage and rest on a fulcrum between the four-bar linkage and the wing. The fulcrum would have several functions; first, the fulcrum would reverse the coupler curve created by the four-bar linkage, second, it would amplify the curve at the tip of the wing because the length between the fulcrum and the wing tip would be several times longer than the length between the fulcrum and the four-bar, third, the fulcrum would provide support for the wing.

In order to generate proper motion and limit forces on the wing-bone, a linkage capable of rotating in all directions and translating the motion of the four-bar linkage was necessary. The MQP team decided that either a universal joint or a ball joint would best suit this application, as this joint would need to best simulate that of the shoulder on a bird and translate the desired wing stroke pattern created by the coupler curve. The group decided that the universal joint was the best choice for a number of reasons, first, because it would have fewer limitations in its motion, second, because it would be capable of absorbing more unwanted forces, and third, because it would not generate as much friction within the joint.

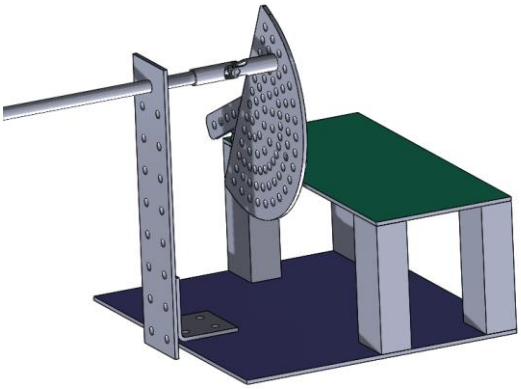

FIGURE 5 CAD MODEL OF ORIGINAL TESTBED DESIGN

3.3 Small-Scale Prototype

The MQP team created a proof-of-concept prototype to ensure the motion would behave as expected. The simple prototype was built at half the scale of the final mechanism, and utilized a hand-crank to replicate the motion without an electric motor. The four-bar linkage on the prototype was made of laser-cut plastic. Issues that were noted in this stage of the design process included: size tolerances of the holes, hardware becoming loose with wear, and insufficient bushings on the axles. These issues all culminated in a problem referred to colloquially as wobbling of the entire four-bar linkage system. The overall system worked as expected.

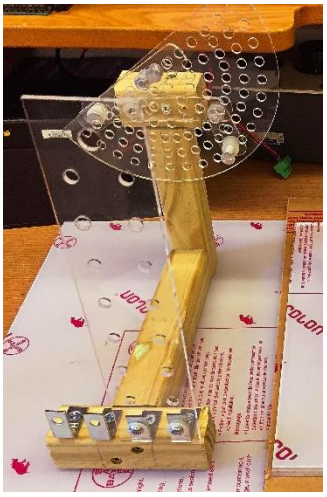

FIGURE 6 PROOF OF CONCEPT HALF-SIZED PROTOTYPE

3.4 Full-Scale Model Design

With a successful prototype, similar materials were used to build the full scale mechanism. Taking into considerations the errors, smaller holes were cut in the four-bar linkage assembly, used different hardware such as set screws within a casing around the axles, and increased the number of bushings used for spacing and to reduce friction and excess space. Despite these changes, issues with the wobbling of the system remained and the MQP team decided an enclosure was necessary to reduce this even further.

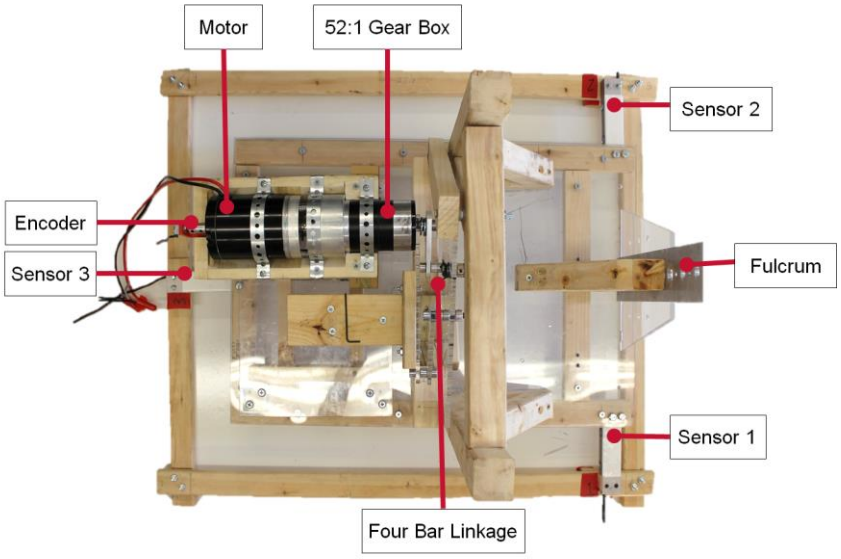

FIGURE 7 PLANFORM VIEW OF FINAL ASSEMBLED TESTBED WITH LABELED FEATURES

Support System

First standing feature with a slot just wider than the width of the protractor was created. It maintained contact during *most* of the rotation. Occasionally, when the rotation caused separation, the protractor attempted to contact again and would collide with the support feature, rather than moving smoothly within the slot. This design was not ideal, instead, a frame was created to provide more support. The new frame has upper supports that maintain constant pressure back toward the motor, while the lower feature presses the four-bar linkage forward toward the wing. This enclosure also maintains two points of pressure in both directions throughout the entire rotation and provides a more stable support system.

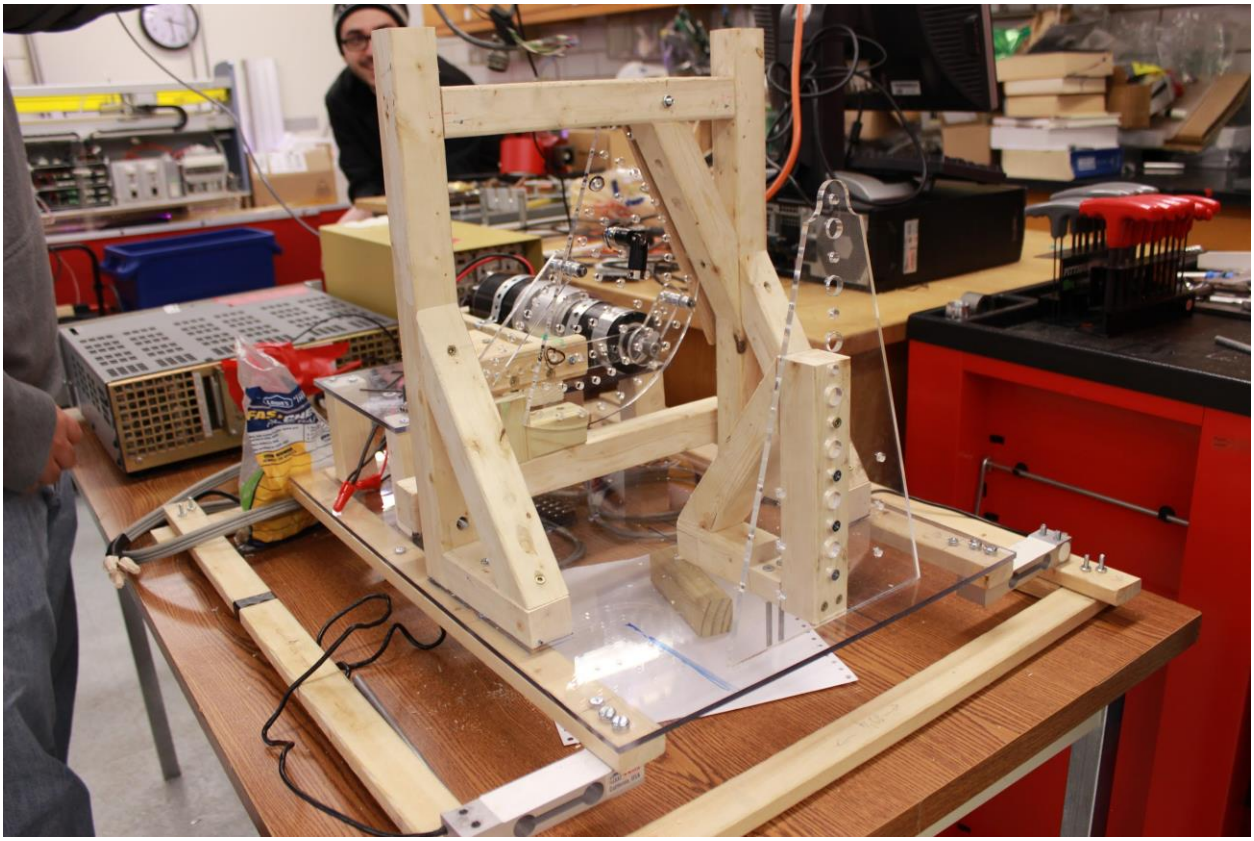

FIGURE 8 IMAGE OF ORNITHOPTER TESTBED FULLY ASSEMBLED

Drive Mechanism

Another issue faced was choosing a motor. The calculations determined that the ideal motor needed to create 50 Nm of output torque at 2 Hz. The team estimated that the torque required would be roughly 20 Nm, therefore 50 Nm yielded a safety factor of 2.5. This was to take into consideration the weight of the wing and general efficiency losses throughout the system. A motor was found in the lab

with a gear ratio of 52:1, it ran at approximately 2 RPM, much slower than the goal of 2 Hz. This led to the conclusion that the MQP team would need to purchase a new motor. The following table shows the comparison of three motors found that would satisfy the power and speed requirements.

TABLE 1 MOTOR SELECTION TABLE

Motor	AmpFlow E30-150	AmpFlow E30-400	AmpFlow F30-150
Price	$79	$109	$199
Peak HP	1	2.1	2.3
RPM	5600	5700	6900
Required Power	31.83 amps at 24V	66.85 amps at 24V	73.21 amps at 24V
Peak Torque	5.01 Nm	10.59 Nm	9.67 Nm

Each of these motors surpassed the necessary torque when geared down to reasonable levels. For the sake of budgeting and available power sources the first option was found to be the best. The MQP team also decided, after some mistakes with purchasing gear boxes, to use the 52:1 planetary gearbox found in the lab. This allows for a maximum speed of 1.79 hertz and a maximum torque of 260.52 Nm, which exceeds our necessary torque requirement while sacrificing some speed. This motor requires a power source capable of 32 amps and 24 volts. Once a power source was obtained, the MQP team was able to assemble the full mechanical system and ensure a working design.

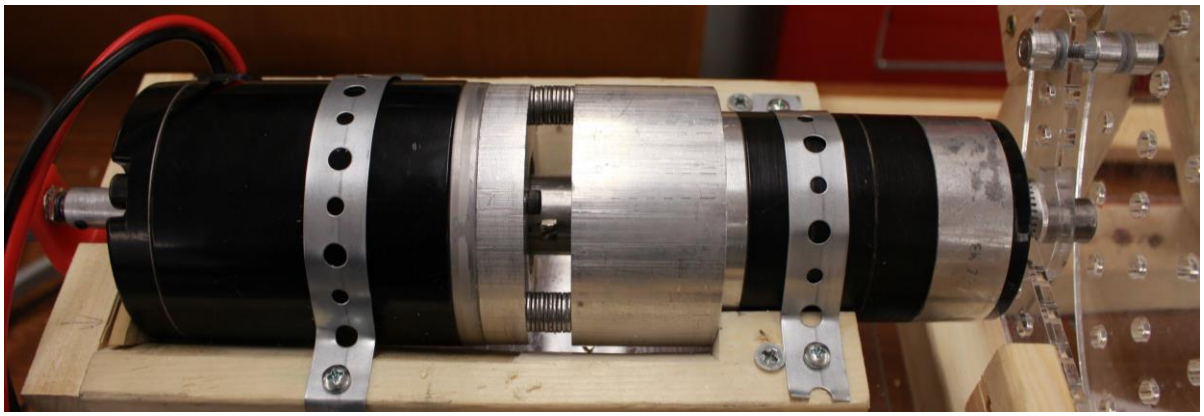

FIGURE 9 PHOTOGRAPH OF DRIVE TRAIN SYSTEM WITH AMP FLOW E30-150 MOTOR AND 52:1 GEARBOX

Wing Design

The wing design was made simple for this MQP's purposes. The group decided to use a rectangular shape with a main cylindrical rod down the center with supporting dowels extending from the rod. The first prototype snapped under pressure. More effort was put into reinforcing the wing. Collars and JB Weld were placed at the intersection of the wing rod and the support dowels. This reinforced the area that was weakened by drilling holes into the main rod. These collars contain features to maintain tension in the parachute fabric.

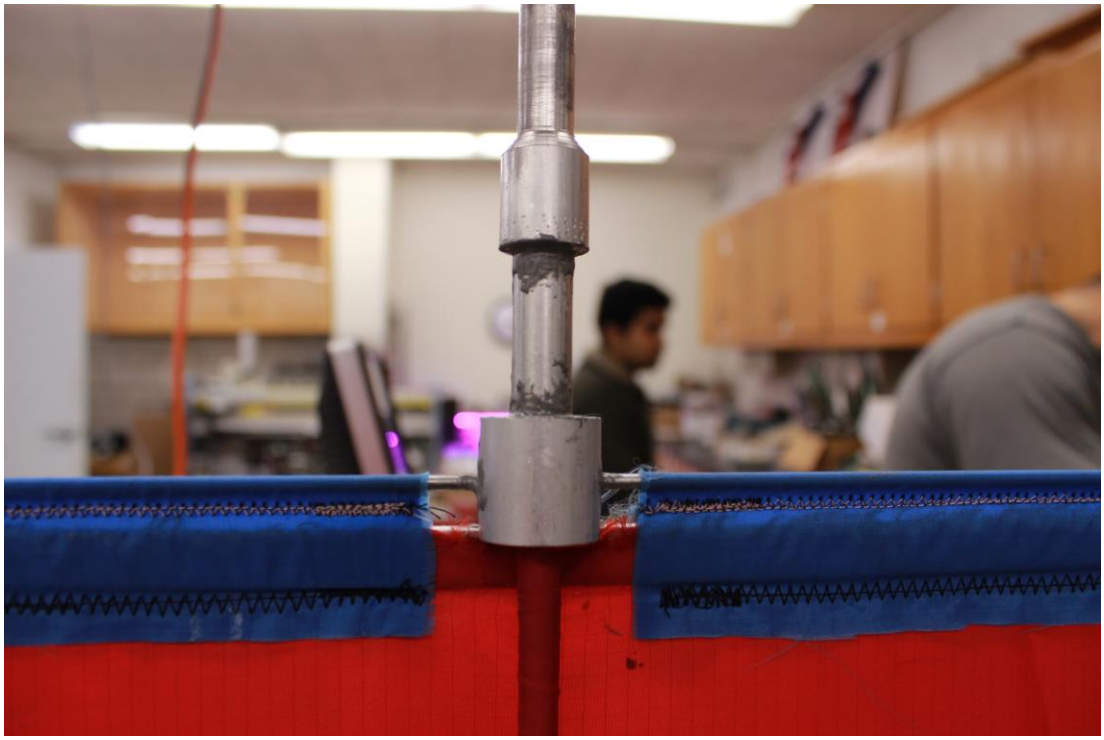

FIGURE 10 IMAGE OF WING-ROD REINFORCEMENTS

With all components built and assembled, initial testing was successful. This, again, showed areas for improvement. The fulcrum component was reinforced with aluminum after exhibiting flexion under the load of the moving wing. The platform that the motor sat on swayed during operation, it was reinforced with a rigid internal frame.

Measurement Devices

Sensors were attached to the platform in order to calculate the force produced by the wing. Three load cells, an encoder, and an inertial measurement unit (IMU) were used. The load cells were placed in a triangular shape. Two load cells were attached to the platform near the wing, mirroring one another. These sensors measure the deflection of the platform at a position closest to the wing. Ideally, these would measure the most accurate force produced by the wing. The third load cell was placed in the center of the platform behind the mechanical mechanism. Its purpose is to measure the displacement longitudinally through the platform.

FIGURE 11 PHOTOGRAPH OF SENSOR ATTACHED TO THE TESTBED

An encoder was placed on the input of the motor. The encoder used was a CUI C14 series panel mount encoder. The encoder is used to determine the rotational position. In this configuration, the

encoder measurs only the falling edges of the rotation. Therefore the encoder clicks “on” with the leading edge and “off” with the trailing edge. Since only the trailing edges were measured, only half of the data was recorded so the total number of clicks had to be multiplied by two in order to represent accurate data. To show the position of the rotating four-bar linkage, a conversion was calculated to relate the input shaft of the motor to the output shaft of the gear box. The ‘clicks’ were divided by the gear box ratio of 52. This calculation resulted in the finding that each encoder ‘click’ relates to 0.615 degrees of rotation of the four-bar linkage.

Finally, an IMU was placed on the moving wing to negate the inertial forces. The load cells measure the forces from an external reference frame. Therefore, additional information is necessary to find the forces generated by the wing moving in space. Finding the difference between the total force measured by the load cell and the forces calculated using information from the IMU results in the total lift created by the wing. The center of mass of the wing was found, and the IMU was placed in that location. The LORD Microstrain 3DM-GX3-45 IMU was lent to the MQP team by an employee, Seth Pierson. The IMU then recorded its accelerometer and gyroscope data. This data, along with the mass of the total wing, were used in Newton’s Second Law to calculate the inertial force.

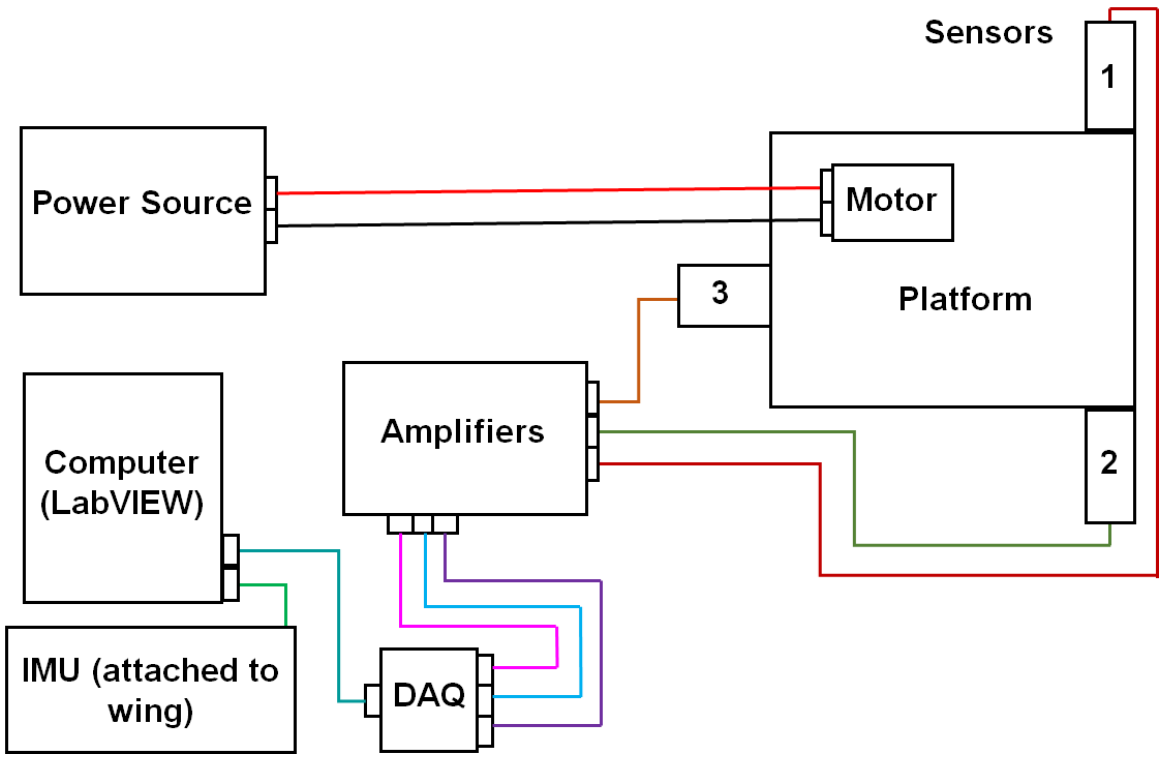

FIGURE 12 TESTBED WIRING SCHEMATIC

LabVIEW Integration

The sensor array sends data to the LabVIEW program on a computer. First the voltage difference from the load cells pass through an amplifier with the gain set to 500. This information goes into the 14-bit Data Acquisition block NI USB-6009

In order to calibrate the load cells, and make useable conclusions from the data, known forces were applied to the sensors. The MQP team continued this for one to six newtons. Using the resistance change recorded by LabVIEW, a conversion factor from voltage to newtons was found. 100 data samples were taken with each force applied. This data was exported to Excel and an average per force was taken. A graph of average velocity versus force was created and a best-fit linear trend line was calculated for each sensor. An example of the results can be seen below.

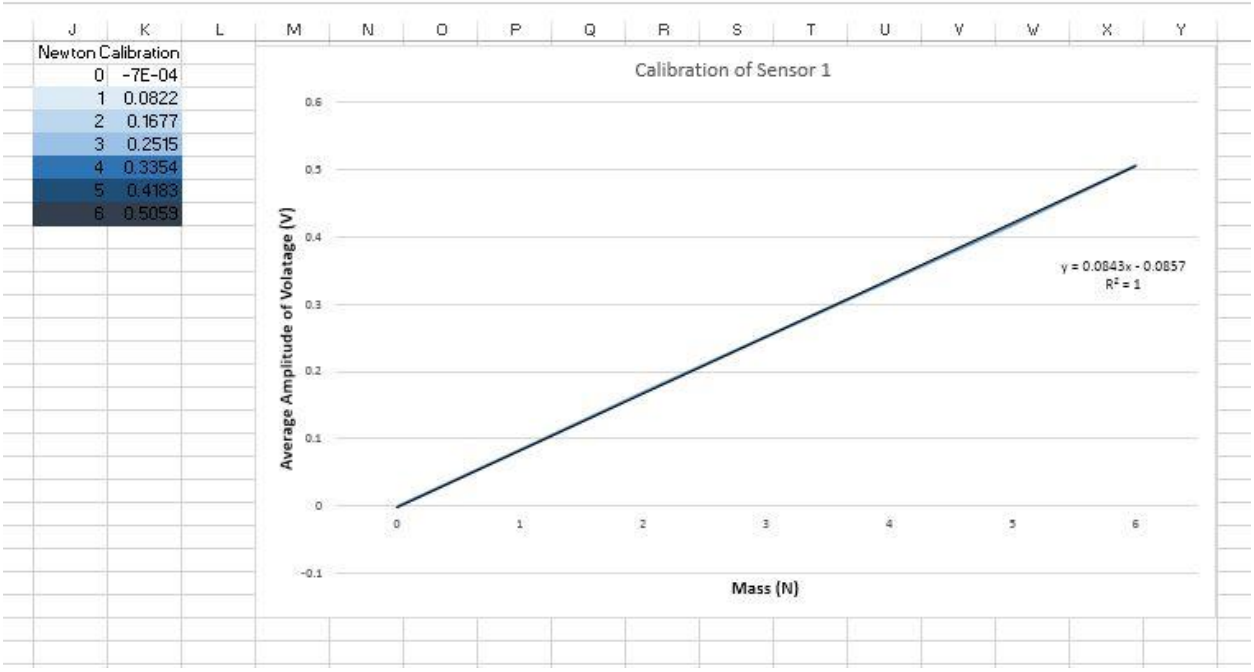

FIGURE 13 EXAMPLE OF SENSOR CALIBRATION DATA

The calculated conversion was then placed into one of the modules of the LabVIEW code. Notice in the figure below, the slope and x-intercept of the graph above are used in the calculations out of the first array. With a few adjustments, the resulting graphs showed results in terms of newtons rather than velocity changes through the load cells.

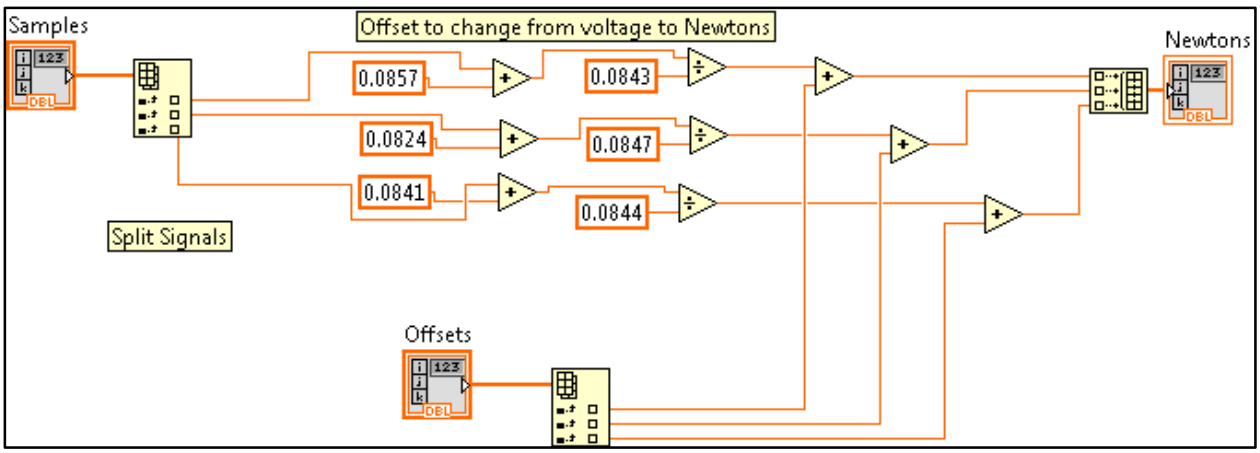

FIGURE 14 LABVIEW MODULE CONVERTED VOLTAGE CHANGE TO FORCE IN NEWTONS

The image below is the main VI of the LabVIEW program. The program was separated into three modules: encoder sample collection, load cell sample collection, and altitude and heading reference system (AHRS) data collection from the IMU. These modules were supplemented with additional 'helper' block diagrams as well. More detailed looks into these modules are found in APPENDIX B: Additional LabVIEW Modules. The main VI calls the modules and aggregates the data in real time.

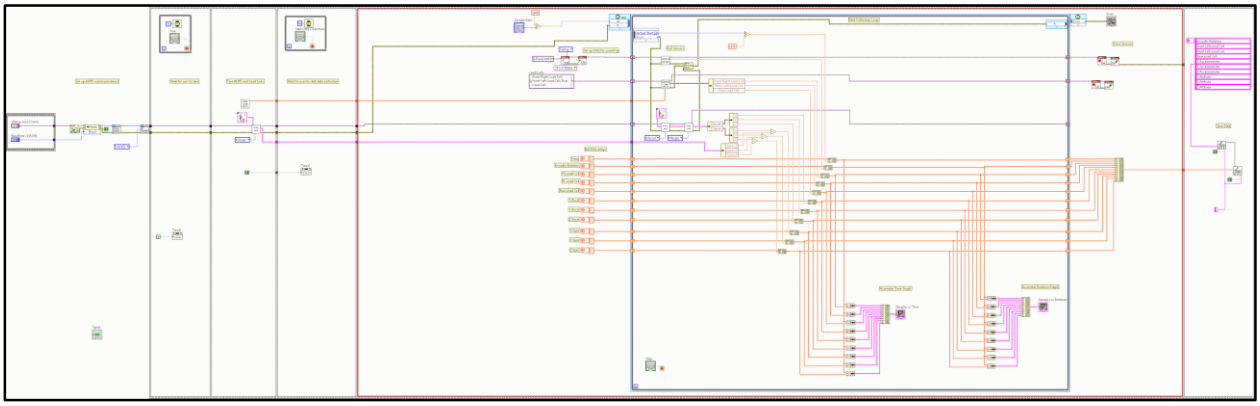

FIGURE 15 IMAGE OF LABVIEW USED TO COLLECT FORCES AND LOCATION POSITION

The front panel of our LabVIEW VI shows two graphs: the plots with reference to time and the plots with reference to rotation. When collecting data, nine lines of data were simultaneously overlaid onto the two graphs. The legend to the right of the graphs illustrates the information available. The front panel was also used to initialize sensors, tare offsets, and data collection. For these experiments, data was collected until the user pressed stop, rather than for a designated number of samples.

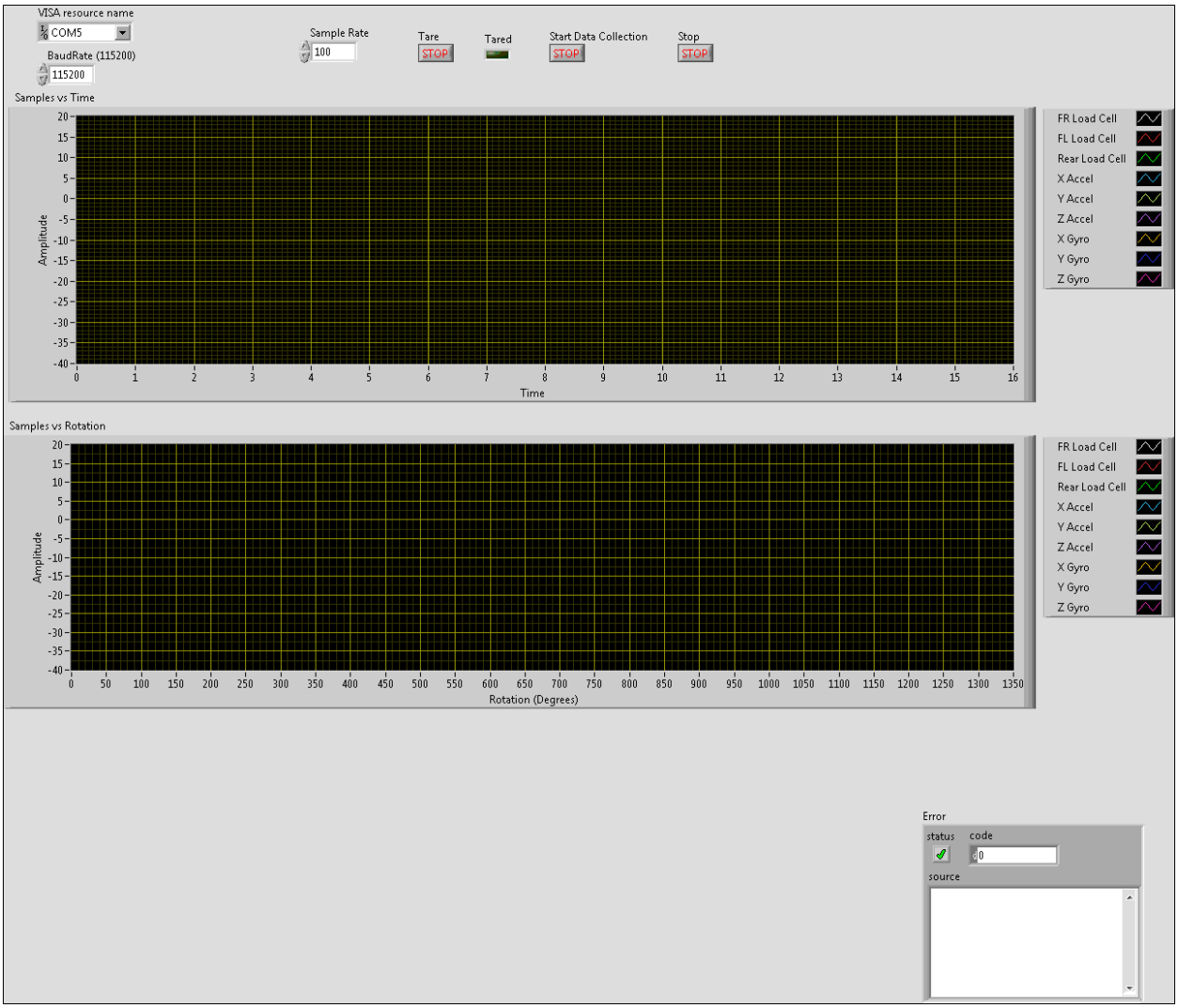

FIGURE 16 FRONT PANEL OF LABVIEW PROGRAM

Chapter 4: Experimental Procedure

The MQP group created a procedure for data collection that simultaneously tested the structural capabilities of the testbed. Lower voltages supplied to the motor outputted lower speeds of the wing. Data was gathered for each curve at a low voltage, in this case six volts, to ensure that the test platform was capable of running the test without breaking. After the six volt tests were successful and no destructive failures occurred, the tests were run again at eight volts. The data was then transferred to an excel spreadsheet where the forces were compared by degree of rotation to compare the characteristics of each curve. Graphs showing multiple periods were generated in order to analyze and compare the coupler curves. The data was also analyzed to obtain the total lift force generated in each curve during a full rotation, during its upstroke, and during its down stroke.

The information collected included data from all of the load cells, the x-, y-, and z- accelerations and the x-, y-, and z- degrees per second measured by the gyroscope of the IMU. Many samples recorded noise or near-zero data as the program began recording before the wing was in motion. A shift of the timestamps and the encoder data was necessary to negate any static forces that occurred when the wing was between the static and dynamic phases of motion. The adjustment was made by subtracting the value of the first relevant timestamp (when the wing was finally in motion) from the rest of the times recorded. This procedure was repeated for the encoder data as well. This allowed the relevant time and positional information to start at 0 seconds and degrees, respectively.

The encoder data also needed post-process calibration as well. The MQP team noticed that though the calculations showed a complete rotation, the encoder only read 250 degrees. A small shift of 1.44 had to be applied in order for one rotation of the output shaft to be represented over 360 degrees.

The data that was most relevant to the calculations were the forces from the load cells. The load cells were summed to find the total external forces. The sign of the load cells were inverted to maintain consistent references with the IMU. For example, when a force was applied downward onto the load cell, a positive number was read. However, during the wing down stroke, the platform would bend upwards causing the load cells or read a negative force. The orientation of the IMU read the forces as down ward acceleration was negative also. This change of sign aligned the load cells and IMU to show consistent data.

Then, the mass of the wing was found using a simple force sensor with Logger Pro provided by Professor Fred Hutson. The mass was determined to be 670g with the IMU and LEDs attached. The MQP team noticed that during the resting period, the z- acceleration read approximately -.941 G. While dangling at

rest, the IMU should experience no acceleration. With the assistance of the MQP co-advisor Professor Cagdas Onal of the Mechanical Engineering Department, a conversion factor was found. In order for the IMU to record 0 m/s^2 at rest, the quantity of gravity (-9.81 m/s^2) was divided by the -.941 G. This resulted in a G to m/s^2 conversion of 10.245. Multiplying this value by the z-acceleration data converted all measurements to terms of m/s^2. However, the data still reflected that, at rest, the wing was moving at -9.81 m/s^2. Therefore, the force of gravity (the quantity 9.81 g/m^2) was subtracted from the z-acceleration data to calibrate the resting z-acceleration as zero. The z-component of the acceleration did not constantly measure the vertical acceleration (true z-acceleration), it measured the vertical acceleration with respect to the IMU; however, the IMU was attached to the rotating and pitching wing. So the z-acceleration did not consistently align with gravity. The MQP team calculated the true z-acceleration by considering the trigonometric relationships shown in Figure 17 below using Equation 1.

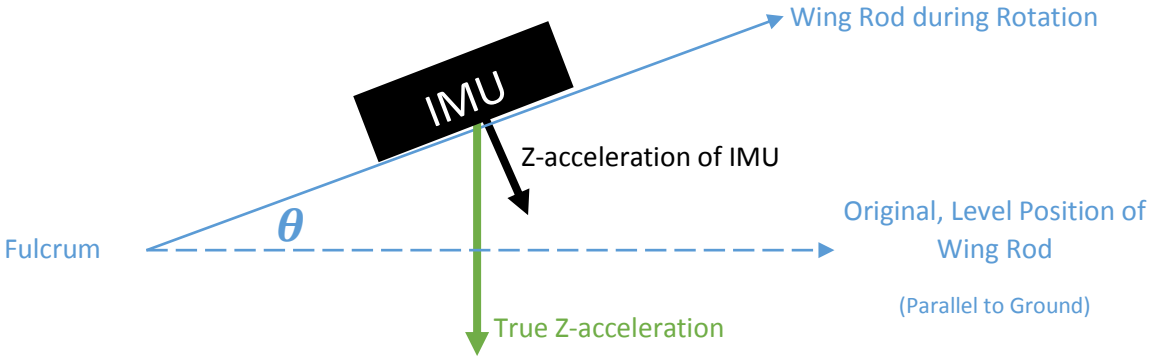

FIGURE 17 TRIGONOMETRIC RELATIONSHIP OF THE VERTICAL ACCELERATION

$$a_{z_{true}} = a_{z_{IMU}} * \cos\theta \quad (1)$$

This equation was then input into the calculations section of the Excel document. The z-acceleration was the data collected from the IMU. The wing angle, θ, is the y-axis gyroscope measured in degrees. The angle was measured as the difference between its original level position and how it pitched within the fulcrum. For Excel to calculate the equation, the gyroscopic measurement was converted to radians. This accounted for the changes in orientation of the IMU. The results of this conversion can be seen more clearly in APPENDIX A: Example of Collected Data.

To find the force of lift, it was necessary to eliminate unnecessary forces at play in the system. One of those forces was the inertial force created by the wing itself and the wing rod. Since the mass of the wing at the z-acceleration were found, Newton's Second Law (force equals mass times acceleration) was used to find the inertial forces at each sample time. Subtracting the inertial forces from the total forces detected from the load cells, the lift generated was calculated.

Chapter 5: Results and Discussion

5.1 Results

The following images show a “light painting” long exposure photograph of the wing at the three designated coupler curves. These graphs were placed side by side to give a visual representation of the forces measured as shown in the figures below. Note that the graphs show the second and third periods of the shaft rotation. These graph show the difference of periods of the three distinct shapes and comparisons of their maximum forces are discernable. The MQP team omitted the first period of wing initially began moving, was not consistent enough for the analysis due to static motion.

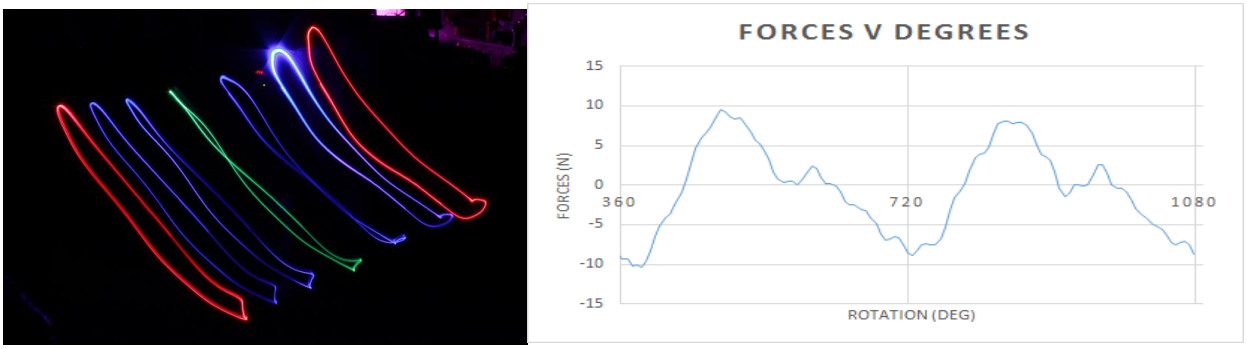

FIGURE 18 FORCES GENERATED OVER MOTOR SHAFT ROTATIONS 2-3 AT POSITION 1

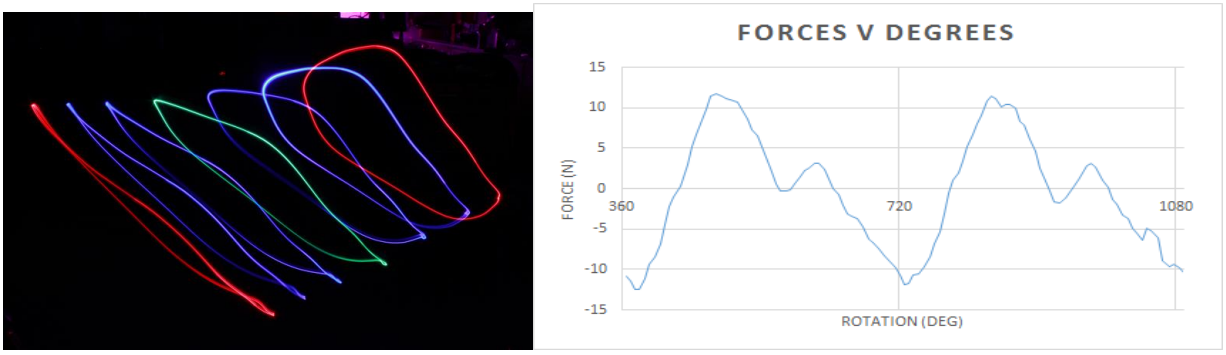

FIGURE 19 FORCES GENERATED OVER MOTOR SHAFT ROTATIONS 2-3 AT POSITION 2

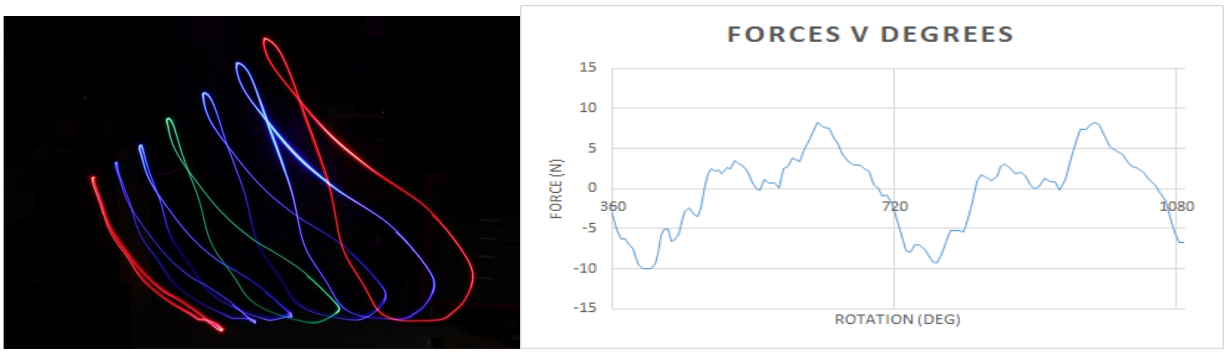

FIGURE 20 FORCES GENERATED OVER MOTOR SHAFT ROTATIONS 2-3 AT POSITION 3

The IMU also collected measurements of the angle of the wing with respect to "level", the starting position which was parallel with ground. The y-gyroscope recorded the angles in degrees. The following graphs show the forces that correspond with the angle of the wing with respect to ground. This demonstrates the different forces created on the up and down strokes. For all graphs, lift is the positive force while upstroke drag is negative. Wing angle is negative during the down stroke of the wing as it is producing the most positive force. As the angle approaches the "extremes" of the graph (the highest and lowest angles), the largest forces are created. This shows that as the wing is at its up and down apexes, the most force is generated.

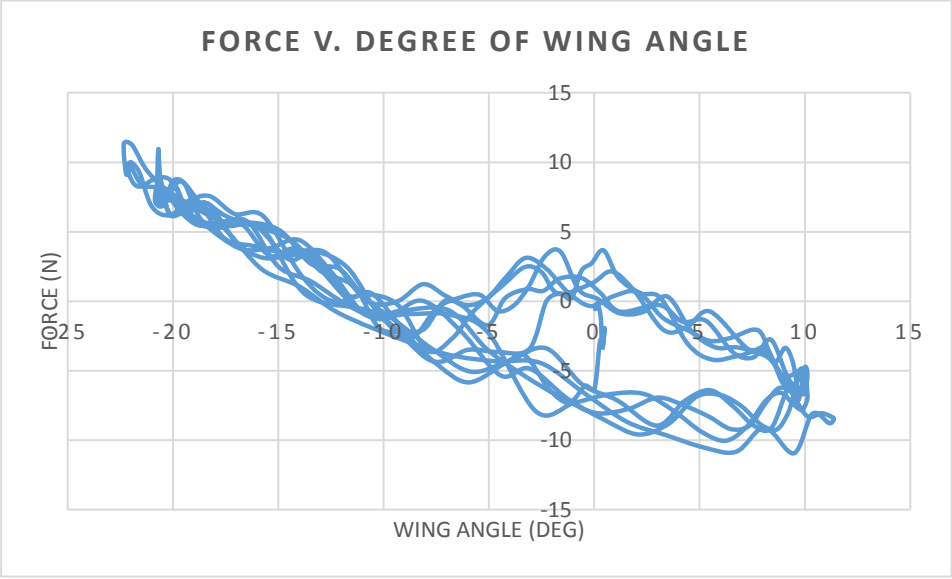

FIGURE 21 FORCE V. DEGREE OF WING ANGLE FOR FIVE PERIODS FOR POSITION 1

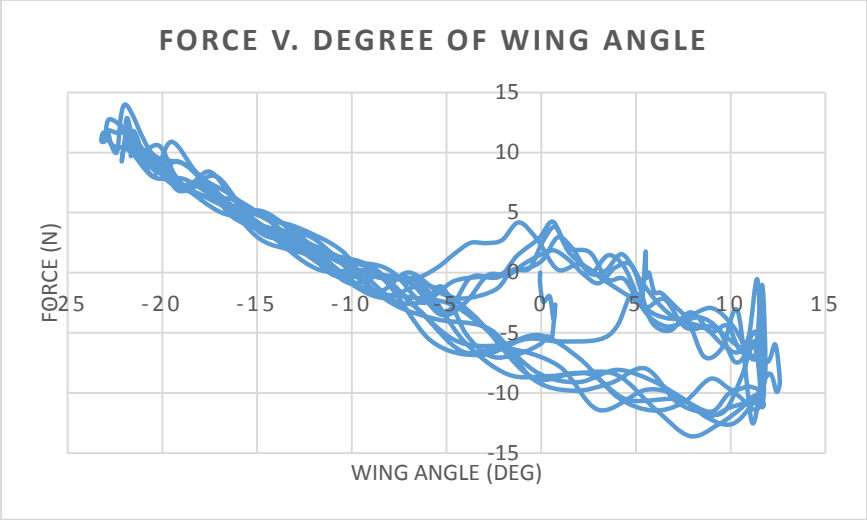

FIGURE 22 FORCE V. DEGREE OF WING ANGLE FOR FIVE PERIODS FOR POSITION 2

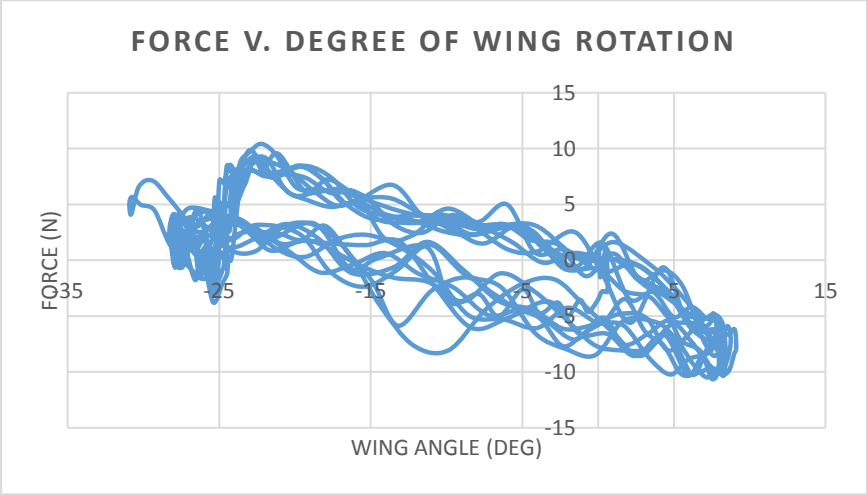

FIGURE 23 FORCE V. DEGREE OF WING ANGLE FOR FIVE PERIODS FOR POSITION 3

Several important characteristics were determined from the collected data illustrated in

Table 2. The maximum force was found for each position. This was the highest numeric value read by the total load cells. The average downforce was measured and refers to the average force achieved during the down stroke of the wing itself for each pattern. The average total force is the combination of the down stroke and upstroke (full rotation) of the wing.

TABLE 2 NOTABLE RESULTS

Flapping Pattern	Maximum Force [N]	Average Downforce [N]	Average Total Force [N]
Position 1	11.34	6.85	-0.635
Position 2	13.99	9.77	-0.29
Position 3	10.42	6.85	-0.189

5.2 Discussions

There are some things to note about the data presented above. The MQP team was most interested in the maximum force produced, the average downwards force, and the average force over the entire periods.

The data collected allowed the team to compare the effectiveness of the coupler curves. From the

Table 2, it can be seen that the second pattern, the teardrop shape, created the highest maximum force and average downforce. Despite this, it also created a significant amount of upward force, referred to as drag. This means that the positive forces, created on the down stroke, were more than negated by the upwards drag. This resulted in an overall negative, albeit small, average total force. This means that lift was not achieved at the test frequency of the wing.

The average total forces of the data was negative for each of the coupler curves studied. Due to the focus placed on creating a working platform prototype, extensive research on wing geometry was not completed. The MQP team attributes the unwanted drag produced during the upstroke to the simple wing design used to evaluate the functionality of the testbed. Further wing design would reduce the drag and thus increase the average total force.

In order to compare the lift achieved by the down stroke, the team focused on the average positive forces of the down stroke as an important characteristic. The most successful wing trajectory was Position 3, which mimicked a figure-eight wing pattern reminiscent of a hummingbird. Although, it did not create the largest downforce, it produced the least amount of negative forces per revolution. This led to the smallest negative average total force.

An interesting result the MQP noticed was the accuracy of the load cell measurements. The following graphs represent the data collected and summed by the two front load cells and the difference found when the inertial forces were subtracted from the forces measured by the load cells. The graphs show that, if necessary, the inertial forces are almost negligible and the forces measured by the load cells only can result in a reasonable approximation of the forces generated.

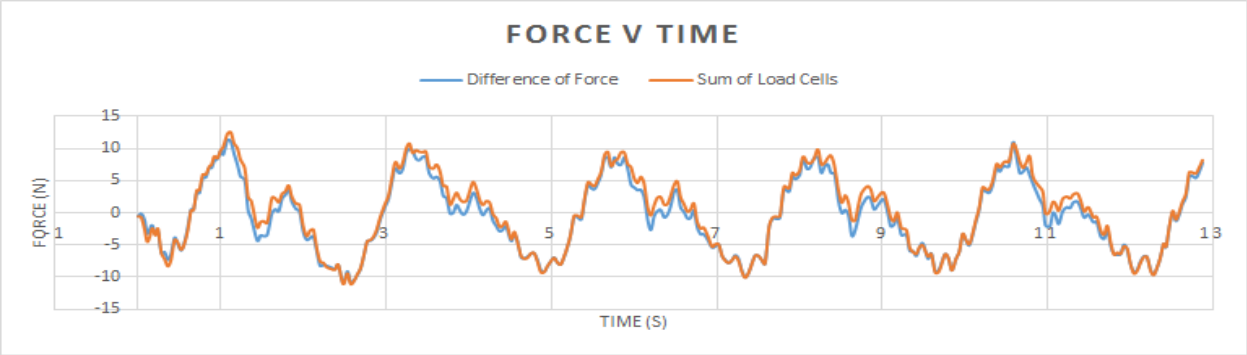

FIGURE 24 CALCULATED TOTAL FORCE V. FORCE MEASURED BY LOAD CELLS AT POSITION 1

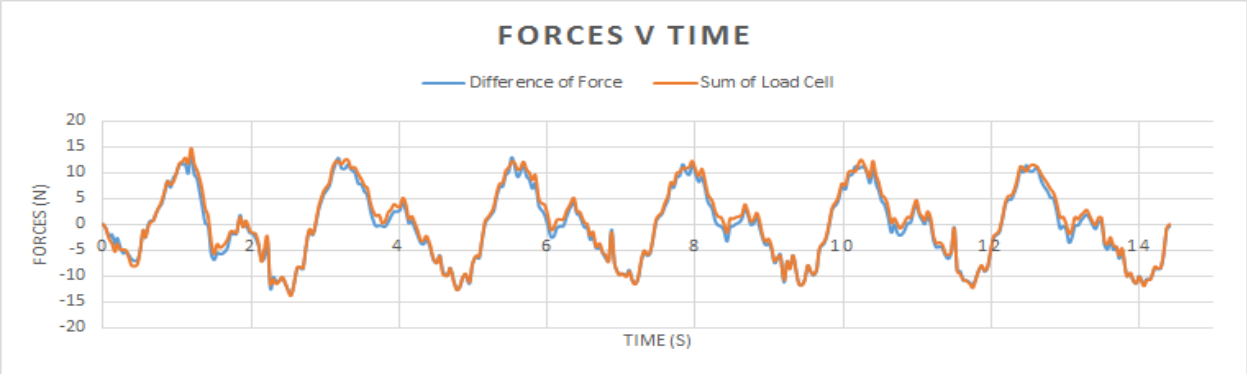

FIGURE 25 CALCULATED TOTAL FORCE V. FORCE MEASURED BY LOAD CELLS AT POSITION 2

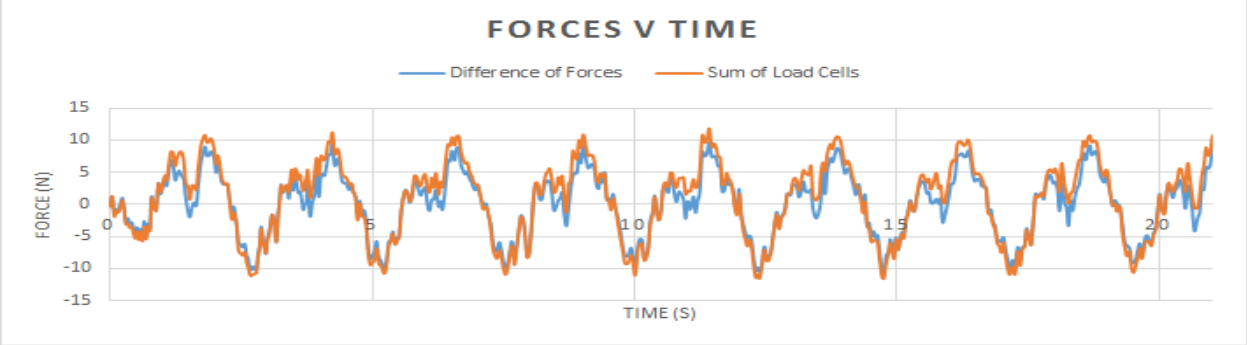

FIGURE 26 CALCULATED TOTAL FORCE V. FORCE MEASURED BY LOAD CELLS AT POSITION 3

Although these results did not produce a wing trajectory that could create a positive average total force with the wing used, the platform overall was successful. The primary goal of the ornithopter testbed was to measure the lift force of a flapping wing. Due to concerns of the deflection of the wing, the loaded platform was not tested at 2 Hz. The data recorded and used for analysis ran at 8 V, this was calculated retroactively to be approximately ½ Hz. The objective of creating a platform that can create multiple flapping trajectories was achieved. The slotted four-bar linkage allows for a broad variety of coupler curves that the team encourages future research of. This also accomplished the third goal: manual adjustability of the platform. To adjust the coupler curves and support fulcrum, only a few screws need repositioning. The culmination of these objectives led to a successful measurement platform that can be used by future teams to test wings and trajectories.

The Ornithopter Testbed MQP team represented Popovic Labs as a feature in the 2015 Cambridge Science Festival (CSF) Robot Zoo. The CSF was an interactive science fair that allowed members of the community to learn and explore regional robotics projects. During this event the testbed operated continuously for four hours at a low power setting. The only consequence of running the testbed for this length of time was heat produced by the motor. Fortunately, the motor never got hot enough to raise any concern. The MQP team observed that the mechanism was capable of producing flapping motion for an extended period of time. The biologically inspired wing movement captured the attention of the audience.

FIGURE 27 MQP TEAM EXPLAINED ORNITHOPTER TESTBED TO CSF PATRONS

FIGURE 28 YOUNG CSF VISITOR MESMERIZED BY FLAPPING WING

Chapter 6: Conclusions and Recommendation

6.1 Conclusions

The goal of this project was to create a testbed capable of producing and collecting lift forces from a flapping wing with variable wing trajectories. The testbed created is successful in testing lift forces generated by a flapping wing and allows for variable wing trajectories to be tested. With the sensor data gathered the MQP group was able to see which wing pattern was best for the wing design.

6.2 Recommendations

In the future, teams continuing this project or projects with similar intentions should considering the following recommendations. The additions listed below will provide more meaningful data for further research and development of ornithopters.

Consider different materials for the test platform.

Due to time and manufacturability, the MQP team predominantly used acrylic, wood, and polycarbonate. Many pieces of the platform were custom designed and fabricated. Acrylic could be manipulated easily using the laser cutter. Similarly, wood was convenient to use for the supporting framework of several components on the testbed given the available tools. With a working design, these materials could be made of lightweight metals for better mechanical properties. Material, such as aluminum, could be used and, if necessary, cut with a water jet to create any necessary custom shapes. This would result in a sturdier platform that could withstand larger forces and faster speeds.

Optimize the wing design.

Continued research using this testbed would require extra attention to the design of the wing. By creating more forces, the wing and rod would also undergo larger stresses and deformation. This year's MQP was predominantly focused on creating a platform to support and measure the forces acting on the wing. Future research to optimize the shape and size of the wing is encouraged. Wing shape and material should be designed in a way that limits drag produced by the upstroke. Material selection for the wing bone could also be more focused. The hollow aluminum tube seemed an obvious choice, but more research of aluminum alloys and carbon fiber could produce sturdier wings.

Update hardware and Data Acquisition Box.

Due to results found in our data, the MQP team estimated several places where error could occur. Specifically, the DAQ Box - encoder data was troublesome. Several different hypotheses were suggested as to why the information was inconsistent including: encoder being used at faster speeds than intended, 14-bit DAQ Box not registering information fast enough to keep up with encoder, etc. These issues should be taken into consideration should the project continue. Also, a different IMU exists in the lab than the one used for this MQP. In order to use that to acquire data, a NI USB-8451 is necessary in order to process the digital IMU information with SPI and IC^2 protocols. A possible solution which this MQP team did not have time to experiment with is the replacement of the encoder with hardware intended for axel measurements and upgrading the DAQ Box.

Measure force of thrust.

The platform for this MQP was designed predominantly to measure the forces in the vertical direction. This allowed the lift force to be determined. In order to learn more about the physics involved in flapping-winged flight, further research and calculation to measure the thrust is necessary. It would also be worthwhile to take measurements in an environment that simulates forward motion through air. This can be achieved in a wind tunnel, or through the use of a large fan in a controlled environment.

Bibliography

[1] Clegg, B., 2013, "Roger Bacon: The First Scientist," Roger Bacon: The First Scientist, Brown Book, Little.

[2] Vinci, L. d., 1506, "Codex on the Flight of Birds," http://airandspace.si.edu/exhibitions/codex/.

[3] Rubin, L., and Leah, R., 2015, "BIOMIMICRY," School arts, 114(7), p. 38.

[4] 2014, "Biomimicry Institute," http://biomimicry.org/.

[5] Biewener, A. A., 2011, "Muscle function in avian flight: achieving power and control," Philosphical Transactions of The Royal Society(366), pp. 1496-1506.

[6] Tucker, V. A., and Parrott, G. C., 1970, "Aerodynamics of Gliding Flight in a Falcon and Other Birds," Experimental Biology(52), pp. 345-367.

[7] Noll, P., "Bird Muscle System," http://www.paulnoll.com/Oregon/Birds/Avian-Muscle.html.

[8] Woodford, C., 2000, "Helicopters," http://www.explainthatstuff.com/helicopter.html.

[9] Woodford, C., 2009, "Airplanes," http://www.explainthatstuff.com/howplaneswork.html.

[10] Billingsley, D., Slipher, G., Grauer, J., and Hubbard, J., 2009, "Testing of a Passively Morphing Ornithopter Wing," The American Institute of Aeronautics and AstronauticsSeattle, Washington.

[11] Harmon, R. L., 2008, "Aerodynamic Modeling of a Flapping Membrane Wing Using Motion Tracking Experiments," Masters of Science, University of Maryland.

[12] Beando, A. O., Pietri, C., Chung, T., and J. Ramirez, K., 2014, "Theoretical Model and Test Bed for the Development and Validation of Ornithopter Designs," Worcester Polytechnic Institute.

APPENDIX A: Example of Collected Data

TABLE 3 EXAMPLE DATA OF THE FIRST 3.55 SECONDS OF COLLECTION AT 8V OF POSITION 1.

Data Measured from Sensors with Conversions																		Calculated Measurements			Results
Time [s]	Adjusted Time [s]	Encoder [clicks]	Adjusted Encoder	FR Load Cell [N]		FL Load Cell [N]		Rear Load Cell [N]	X Accel [g]	Y Accel [g]	Z Accel [g]	Z [m/s^2]	X Gyro	Y Gyro	Z Gyro	Y Gyro [rad]	mass [kg]	Adjusted Calculated Force	Sum of Load Cells [N]	Difference of Forces [N]	Average Force Over 1 Rotation
2.77	0	0	0	-0.62	0.62	1.189	1.189	-0.453	0.303	0.19	0.939	0	-0.018	0.041	-0.095	0.000715585	0.675	0	-0.569	-0.569	-0.48642243
2.81	0.04	1.731	2.49264	-0.06	0.06	0.813	0.813	0.151	0.334	0.142	1.023	0.877571885	0.007	0.157	-0.07	0.002740167		0.592358798	-0.753	0.160641202	
2.85	0.08	5.192	7.47648	1.089	-1.089	1.61	-1.61	-0.951	0.343	0.058	-1.153	-2.23571885	-0.11	0.311	0.053	0.005427974	gravity conversion	-1.509087992	-2.699	-1.189912008	Average Force over 2 Rotations
2.88	0.11	8.221	11.83824	0.559	-0.559	3.958	-3.958	-2.688	0.34	0.097	1.12	1.890958466	-0.446	0.366	0.206	0.006387905	10.44728435	-1.276370923	-4.517	-3.240629077	-0.456821024
2.91	0.14	11.25	16.2	0.06	-0.06	3.687	-3.687	-3.549	0.368	0.155	-1.109	1.776038339	-0.908	0.447	0.465	0.007801622		-1.198789395	-3.747	-2.548210605	
2.94	0.17	14.279	20.56176	-1.24	-1.24	3.627	-3.627	-1.692	0.359	0.053	-1.005	0.689520767	-1.428	0.495	0.989	0.00863938	encoder conversion	-0.465409148	-2.387	-1.921590852	Average Force Over 3 Rotations
2.98	0.21	18.173	26.16912	-0.363	-0.363	3.868	-3.868	-3.715	0.347	0.007	0.96	0.219392971	-1.45	0.406	1.953	0.007086037	1.44	-0.148086538	-3.505	-3.356913462	-0.511989485
3.01	0.24	21.202	30.53088	-0.469	-0.469	2.95	-2.95	-3.051	0.343	0.025	-0.888	0.532811502	-1.311	0.278	2.836	0.004852015		0.35964353	-2.481	-2.84064353	
3.05	0.28	25.529	36.76176	-1.361	-1.361	4.831	-4.831	-4.818	0.328	0.051	-0.924	0.156709265	-1.108	0.011	4.312	0.000191986	gravity (m/s2)	-0.105778752	-6.192	-6.297778752	Average Force Over 2-3
3.09	0.32	29.423	42.36912	-2.903	-2.903	4.259	-4.259	-4.788	0.365	0.068	-1.093	1.608881789	-0.963	-0.42	6.129	0.007330383	9.81	1.08596603	-7.162	-6.07603397	-0.525310136
3.13	0.36	33.317	47.97648	-4.113	-4.113	4.199	-4.199	-3.957	0.373	0.106	-1.082	1.493961661	-0.135	-1.199	8.095	0.020926498		-1.008203326	-8.312	-7.303796674	
3.17	0.4	37.644	54.20736	-4.914	-4.914	2.333	-2.333	-3.308	0.341	0.217	-1.068	1.347699681	0.811	-2.132	10.081	-0.03721042		-0.909067567	-7.247	-6.337932433	Average Force Over 2-5
3.21	0.44	41.538	59.81472	-3.992	-3.992	0.241	-0.241	-2.311	0.31	0.233	-0.985	-0.48057508	1.483	-3.289	12.09	0.057403879		-0.323853863	-4.233	-3.909146137	-0.634516835
3.24	0.47	44.567	64.17648	-4.672	-4.672	0.316	-0.316	-2.326	0.275	0.23	-0.921	0.188051118	2.154	-4.25	13.534	0.074176493		-0.126585458	-4.356	-4.482585458	
3.29	0.52	49.76	71.6544	-7.182	-7.182	1.445	-1.445	-3.202	0.25	0.31	-0.925	0.146261981	3.738	-5.94	15.594	0.103672558		-0.098196754	-5.737	-5.835196754	Max Force
3.33	0.56	54.087	77.88528	-7.515	-7.515	2.754	-2.754	-2.356	0.215	0.345	-0.96	0.219392971	5.439	-7.394	16.922	0.129049645		-0.146858832	-4.761	-4.614141168	11.34371979
3.37	0.6	57.981	83.49264	-6.789	-6.789	4.018	-4.018	0	0.176	0.3	-1.002	0.658178914	7.361	-8.933	17.975	0.155910262		-0.438882027	-2.771	-2.332117973	
3.41	0.64	62.308	89.72352	-5.791	-5.791	6.125	-6.125	1.238	0.14	0.288	-0.968	0.302971246	8.677	-10.525	18.603	0.183695904		-0.201064846	0.334	0.535064846	Average Downstroke of 2 and 3
3.44	0.67	65.337	94.08528	-5.806	-5.806	6.231	-6.231	1.374	0.107	0.32	-0.942	0.031341853	9.066	-11.738	18.767	0.204866748		-0.020713344	0.425	0.445713344	Rotation 2
3.48	0.71	69.663	100.31472	-4.128	-4.128	7.645	-7.645	1.616	0.073	0.326	-0.906	0.344760383	8.85	-13.351	18.588	0.233018908		-0.226423884	3.517	3.290576116	7.158426636
3.51	0.74	72.692	104.67648	-3.704	-3.704	7.164	-7.164	2.567	0.046	0.336	-0.876	0.658178914	8.502	-14.523	18.181	0.253474167		-0.430075007	3.46	3.029924993	Rotation 3
3.55	0.78	76.587	110.28528	-1.346	-1.346	7.269	-7.269	2.915	0.012	0.279	-0.859	0.835782748	7.623	-16.051	17.352	0.280142798		-0.542160381	5.923	5.380839619	6.548911358
3.59	0.82	80.913	116.51472	-0.438	-0.438	6.381	-6.381	3.881	0.004	0.242	-0.879	0.626837061	5.944	-17.494	16.262	0.305327899		-0.403545284	5.943	5.539454716	Total
3.63	0.86	84.808	122.12352	-0.983	-0.983	6.201	-6.201	3.836	0.034	0.183	-0.913	0.271629393	2.582	-18.85	15.102	0.328994564		-0.173516361	7.184	7.010483639	6.853668997
3.66	0.89	88.269	127.10736	-2.177	-2.177	5.343	-5.343	4.727	0.034	0.231	-0.862	0.804440895	-0.212	19.812	14.179	0.345784631		-0.510857469	7.52	7.009142531	

a

3.69	0.92	91.298	131.46912	-3.704	3.704	-5.072	5.072	5.89	-0.049	0.262	-0.836	1.076070288	-3.013	-20.585	13.223	-0.359276027		0.679971333	8.776	8.096028667
3.73	0.96	95.192	137.07648	-3.931	3.931	-4.56	4.56	5.482	-0.063	0.18	-0.924	0.156709265	-6.043	-21.475	12.175	-0.374809457		0.098435317	8.491	8.392564683
3.77	1	99.519	143.30736	-5.685	5.685	-4.078	4.078	6.313	-0.058	0.166	-0.922	0.177603834	-8.297	-22.011	11.402	-0.384164422		0.111144576	9.763	9.651855424
3.8	1.03	102.548	147.66912	-6.229	6.229	-4.018	4.018	6.343	-0.067	0.094	-0.77	1.765591054	-10.1	-22.218	10.948	-0.387777253		1.103286934	10.247	9.143713066
3.85	1.08	107.74	155.1456	-7.59	7.59	-4.68	4.68	7.355	-0.074	0.114	-0.797	1.483514377	-15.193	-22.33	10.663	-0.389732022		0.926280213	12.27	11.34371979
3.89	1.12	111.635	160.7544	-7.182	7.182	-5.343	5.343	7.355	-0.077	0.168	-0.742	2.058115016	-19.318	-21.935	10.7	-0.382837971		1.288658996	12.525	11.236341
3.93	1.16	115.962	166.98528	-5.05	5.05	-5.749	5.749	6.207	-0.053	0.274	-0.711	2.381980831	-22.459	-21.179	10.994	-0.369643282		1.499237766	10.799	9.299762234
3.97	1.2	120.288	173.21472	-3.931	3.931	-6.095	6.095	7.098	-0.063	0.323	-0.581	3.740127796	-24.862	-19.948	11.406	-0.348158279		2.373117755	10.026	7.652882245
4.01	1.24	124.183	178.82352	-2.238	2.238	-5.945	5.945	6.192	-0.037	0.45	-0.576	3.792364217	-28.509	-17.666	11.895	-0.308329866		2.439127946	8.183	5.743872054

Some things to note about the data above:

The cells shaded green are raw data from LabVIEW. The cells shaded yellow are “adjusted” cells. Their contents were changed minimally for a variety of reasons listed below. The cells shaded blue were used for calculation and graphing.

a. Time is adjusted by 2.7 seconds because for the first 2.7 seconds the wing was static. Data began recording before the wing moved.
b. Encoder is adjusted by a factor of 1.44 to represent a full rotation as 360 degrees.
c. The magnitude of the load cells were inverted to align their directional measurements with the IMU.
d. Z-acceleration was adjusted by the “gravity conversion” then negated by the magnitude of gravity ensure it read zero meters per second squared when at rest.
e. The y-gyro data was converted to radians for trigonometric calculations.

APPENDIX B: Additional LabVIEW Modules

The following LabVIEW Block Diagrams were called by the main VI, Figure 15.

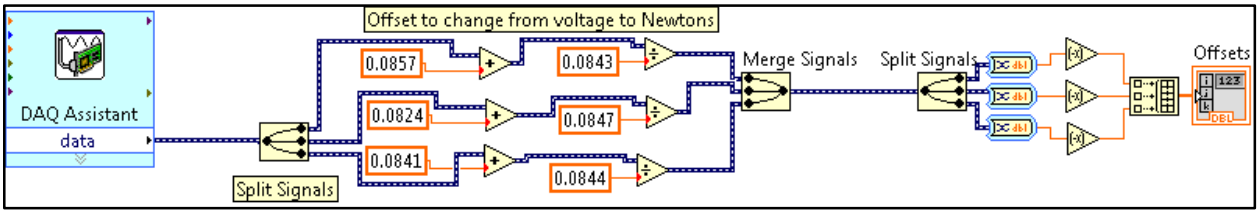

FIGURE 29 TARE SENSORS BLOCK DIAGRAM

Before collecting data, all sensors were set to tare. This zeroed the load cells and the IMU. The user then started the data collection. The main VI called three different modules: Sample Load Cells, Sample Encoder, and Sample 3DM simultaneously at a specified sample rate. Each Sample Block Diagram then asked the respected measurement device for its data at the sample time.

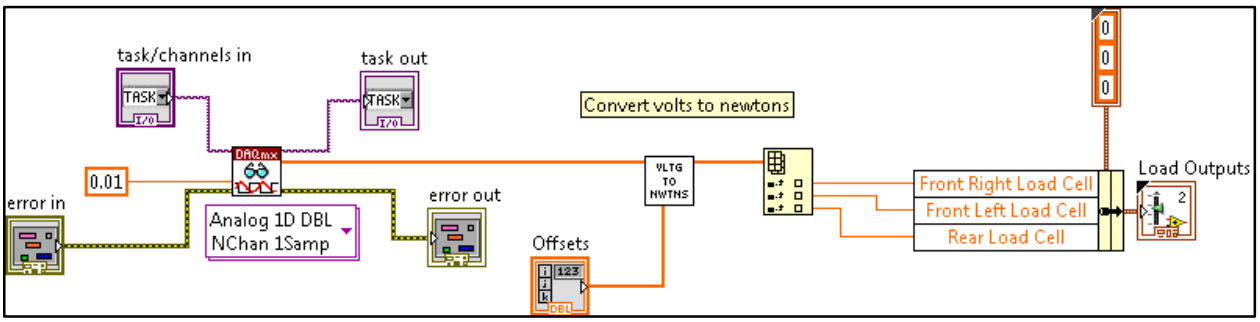

FIGURE 30 SAMPLE LOAD CELLS BLOCK DIAGRAM

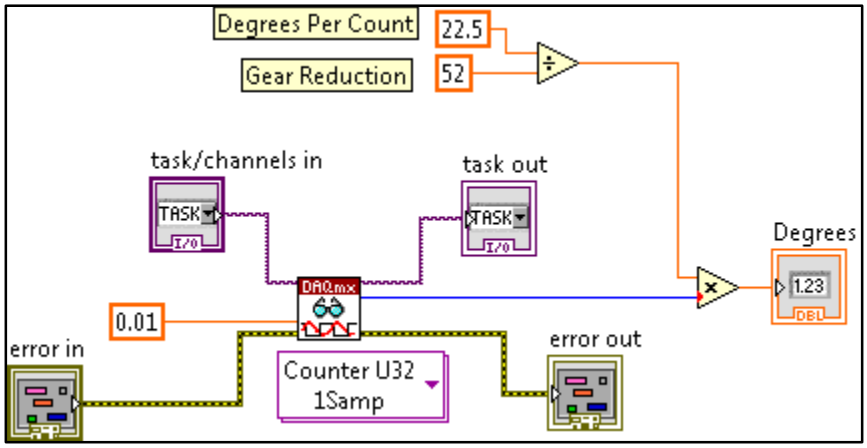

FIGURE 31 SAMPLE ENCODER BLOCK DIAGRAM

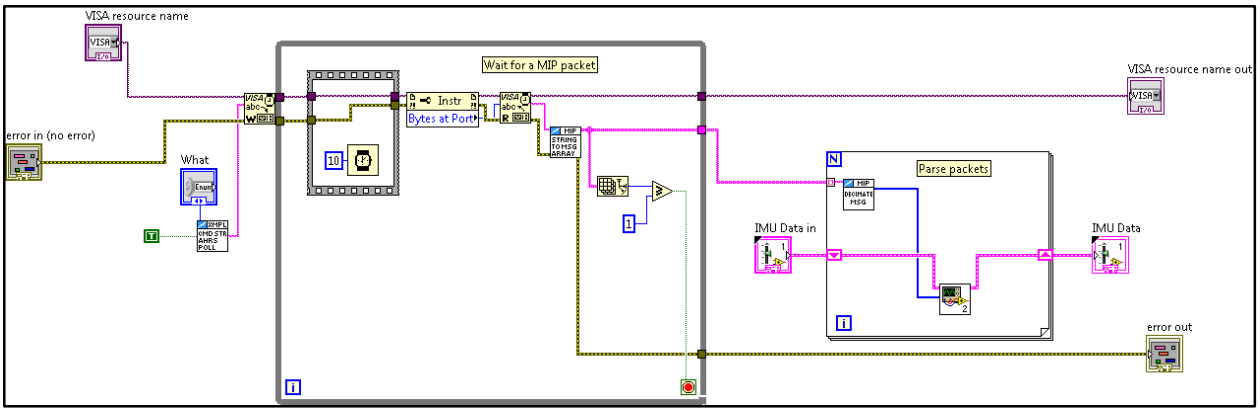

FIGURE 32 POLL 3DM BLOCK DIAGRAM

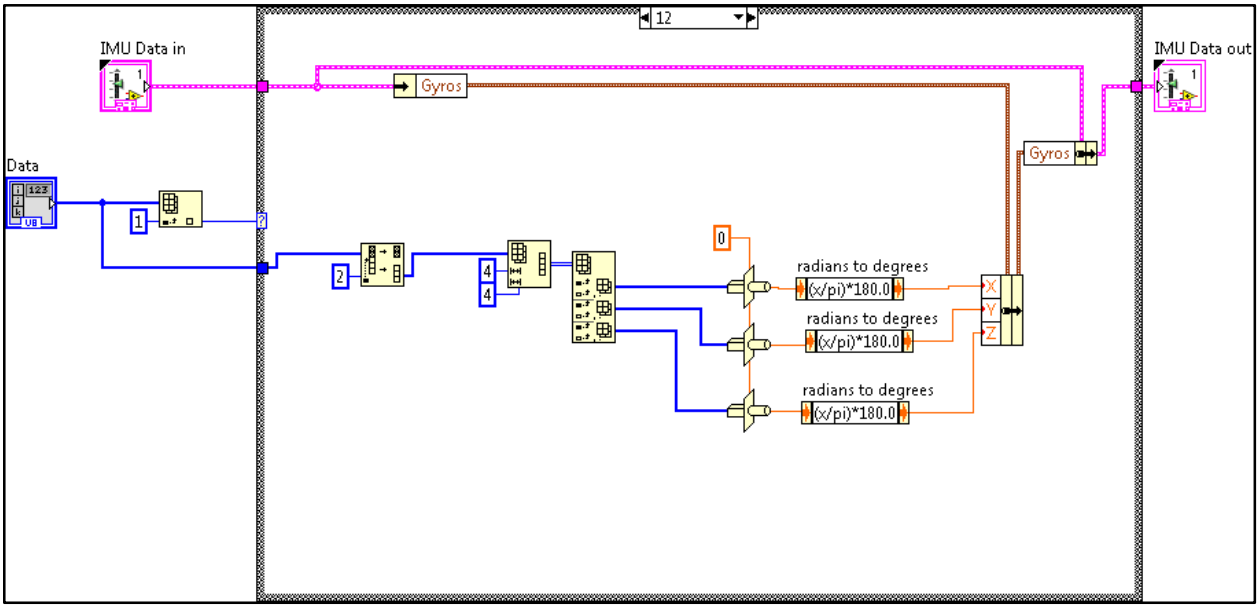

FIGURE 33 PARSE IMU PACKET VI

An additional parsing step was necessary for the data from the IMU. The Poll 3DM Block Diagram "asked" the IMU for the data at the sample time. The IMU then sent a packet of data to the computer. The Parse IMU Packet block diagram then converted the packet into information LabVIEW could use.

This information was then returned to the main VI in Figure 15 which aggregates the information and displays it to the graphs on the Front Panel in real time. To save this information, the graphical data was exported as a CSV file.

APPENDIX C: Additional Representation of Data

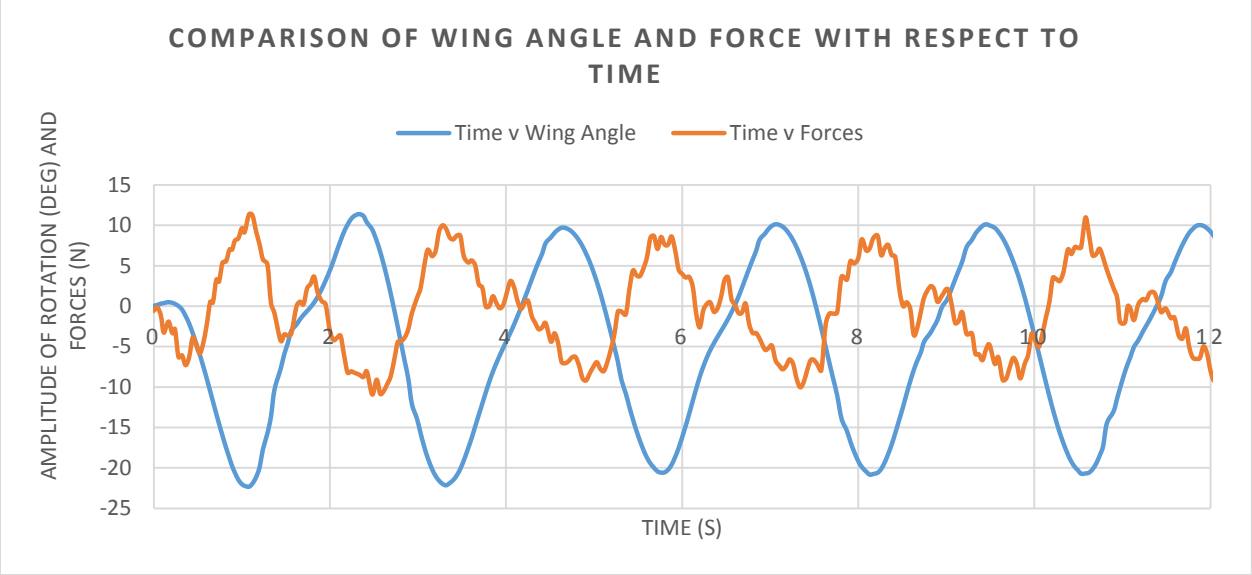

FIGURE 34 WING ANGLE AND FORCE PLOTTED AGAINST TIME FOR POSITION 1

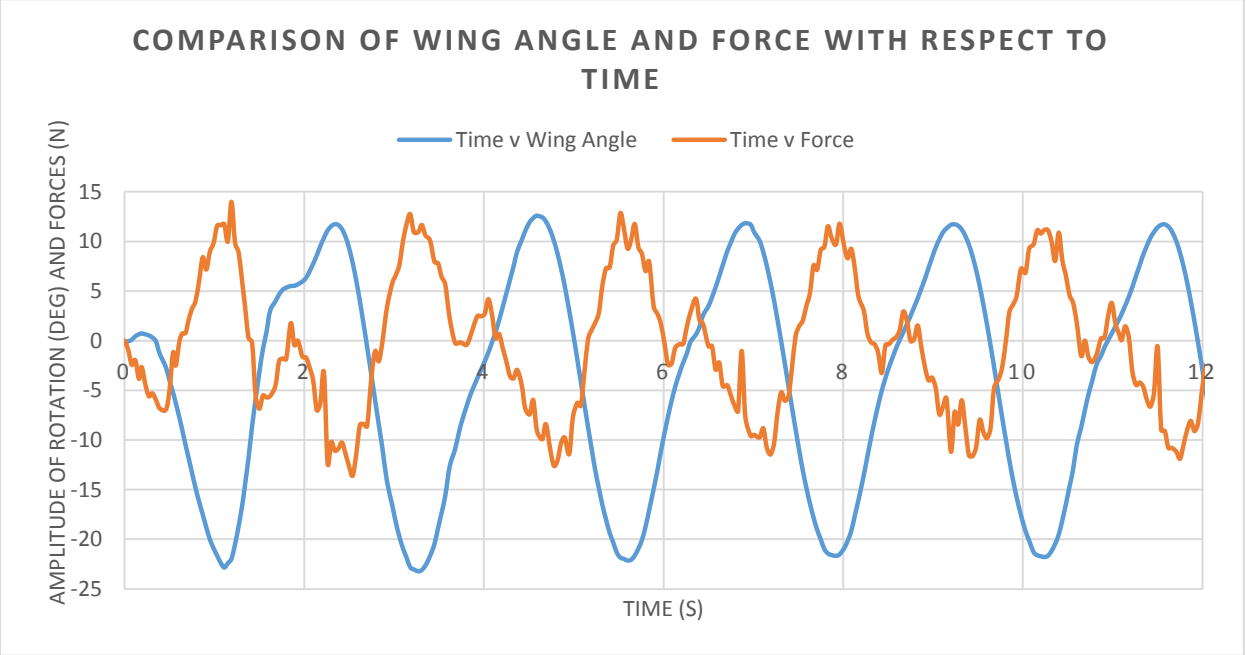

FIGURE 35 WING ANGLE AND FORCE PLOTTED AGAINST TIME FOR POSITION 2

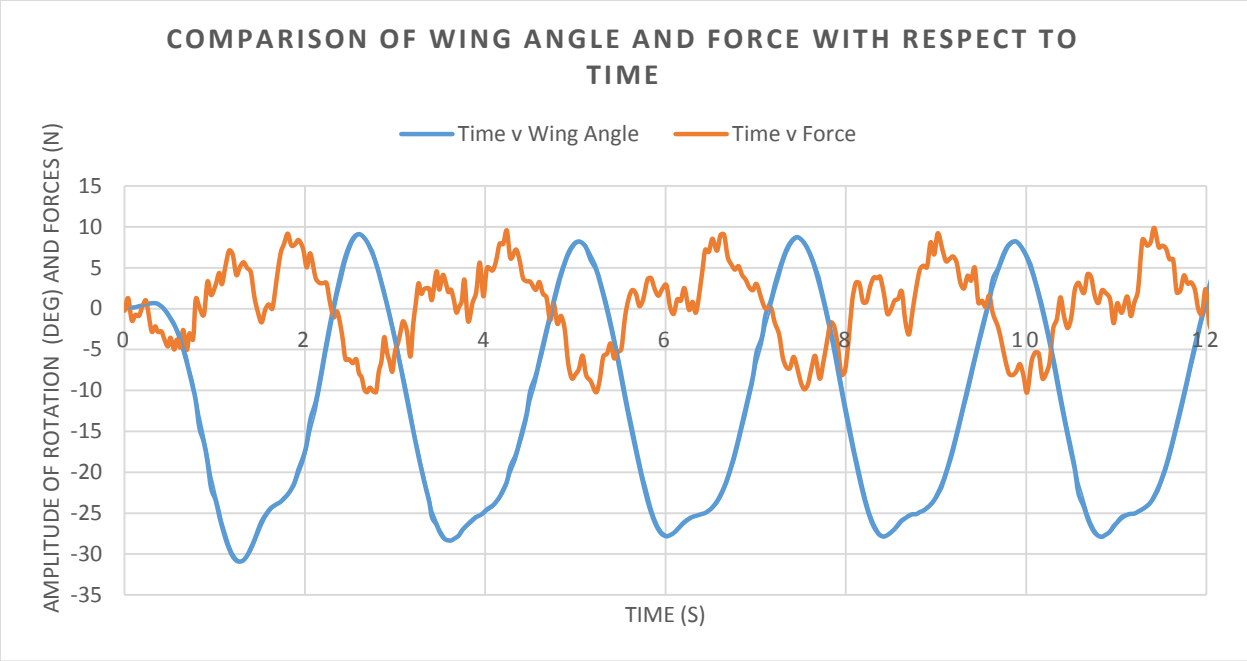

FIGURE 36 WING ANGLE AND FORCE PLOTTED AGAINST TIME FOR POSITION 3

g